Review

Check for updates

Sources of solar energetic particles

Loukas Vlahos[1], Anastasios Anastasiadis[2], Athanasios Papaioannou[2], Athanasios Kouloumvakos[3] and Heinz Isliker[1]

[1]Department of Physics, Aristotle University, Thessaloniki 54124, Greece
[2]Institute for Astronomy, Astrophysics, Space Applications and Remote Sensing, National Observatory of Athens, Penteli 15236, Greece
[3]IRAP, Université de Toulouse III - Paul Sabatier, CNRS, CNES, UPS, Toulouse, France

(iD) LV, 0000-0002-8700-4172; AA, 0000-0002-5162-8821; HI, 0000-0001-9782-2294

Solar energetic particles are an integral part of the physical processes related with space weather. We present a review for the acceleration mechanisms related to the explosive phenomena (flares and/or coronal mass ejections, CMEs) inside the solar corona. For more than 40 years, the main two-dimensional cartoon representing our understanding of the explosive phenomena inside the solar corona remained almost unchanged. The acceleration mechanisms related to solar flares and CMEs also remained unchanged and were part of the same cartoon. In this review, we revise the standard cartoon and present evidence from recent global magnetohydrodynamic simulations that support the argument that explosive phenomena will lead to the spontaneous formation of current sheets in different parts of the erupting magnetic structure. The evolution of the large-scale current sheets and their fragmentation will lead to strong turbulence and turbulent reconnection during solar flares and turbulent shocks. In other words, the acceleration mechanism in flares and CME-driven shocks may be the same, and their difference will be the overall magnetic topology, the ambient plasma parameters, and the duration of the unstable driver.

This article is part of the theme issue 'Solar eruptions and their space weather impact'.

1. Introduction

Solar energetic particles (SEPs) contain important information about the mechanisms of the particle energization inside the solar corona, as well as the properties of the acceleration volume. So far two classes of SEP events are observed and are classified as 'gradual' and 'impulsive'. The two classes have several distinct characteristics. The impulsive events are associated with short time scales, large electron to proton and ^{3}He/^{4}He ratios, and high ionization state, indicating a source region with temperature 3×10^7 K. Gradual events are associated with larger time scales and coronal or interplanetary shocks, high proton intensities, energetic abundances similar to the solar corona, and charge states corresponding to the source region with temperature 3×10^6 K [1]. Classifications are always useful in order to divide events originating from different physical processes. However, observations from advance composition explorer (ACE) spacecraft revealed rich structure in the time dependence of the two classes of SEP. A recent analysis of ACE data indicates that many events defy a simple classification as 'impulsive' or 'gradual'. Gradual events possess an impulsive part, suggesting a clear synergy between flare-accelerated particles with shock acceleration. On the other hand, gradual events related with radio, X-ray and gamma-ray observations indicate that particle acceleration takes place in large-scale coronal structures behind the coronal mass ejection (CME), and that the CME is not the sole acceleration region in gradual events [2].

A theory of particle acceleration in solar flares must explain how electrons and ions are energized out of thermal plasma, as well as providing time scales, energy spectra, fluxes and abundance ratios for various particle species. At the same time, it should address the characteristics of the induced emission of radio waves, X-rays, gamma-rays and neutrons. The current stage of the theory of particle acceleration during solar eruptions is based on a static two-dimensional (2D) picture of the so-called standard cartoon for solar flares (figure 1). In this picture, the acceleration of electrons is based on the reconnection at the current sheet formed below the large-scale CME magnetic structure [4]. The stochastic acceleration of particles by the weak turbulence driven by the jets of the reconnecting current sheet has been analysed in [5].

Alternatives to the above scenario are relying on the evolution and fragmentation of the monolithic current sheet and the re-acceleration of particles in many current sheets formed along the erupting magnetic structure [6]. The stochastic acceleration of ions by weak magnetohydrodynamic (MHD) turbulence serves as the main mechanism for the abundance enrichment mentioned earlier [5,7]. Unfortunately, this mechanism cannot account for the efficient acceleration of ^{3}He and alternative ideas have been proposed in the literature [8,9]. The 'standard' cartoon for solar flares cannot explain the fast escape for the impulsive SEP electrons and ions. Its purpose was to model mainly the radio and X-ray emission from low coronal loops. At the same time, the CME-driven shocks can also efficiently accelerate ions (see the reviews [10–12]).

In this review, we stress two important points: (a) How the photospheric turbulence drives the spontaneous formation of current sheets during solar eruptions (see the brief discussion in §3, where we emphasize the data-driven MHD modelling, and see more details in the article by Archontis & Syntelis [13]), and (b) how the unstable large-scale magnetic topologies sustain strong turbulence, which is crucial for particle acceleration in solar flares and CME-driven shocks. We believe that current data-driven large-scale 3D MHD simulations are closer to a realistic scenario for the acceleration of the SEP [14].

This review is organized as follows: In §2, we outline the main observational constraints on current theories on SEP acceleration theories. In §3, we discuss the evolution of the data-driven large-scale magnetic topologies during an eruption. In §4, we point out the difference between weak and strong turbulence, and in §5, we analyse the acceleration of particles during magnetic flux emergence. In §6, we briefly discuss the mechanisms for particle acceleration in CME-driven shocks, and in §7, we outline the main points of this review.
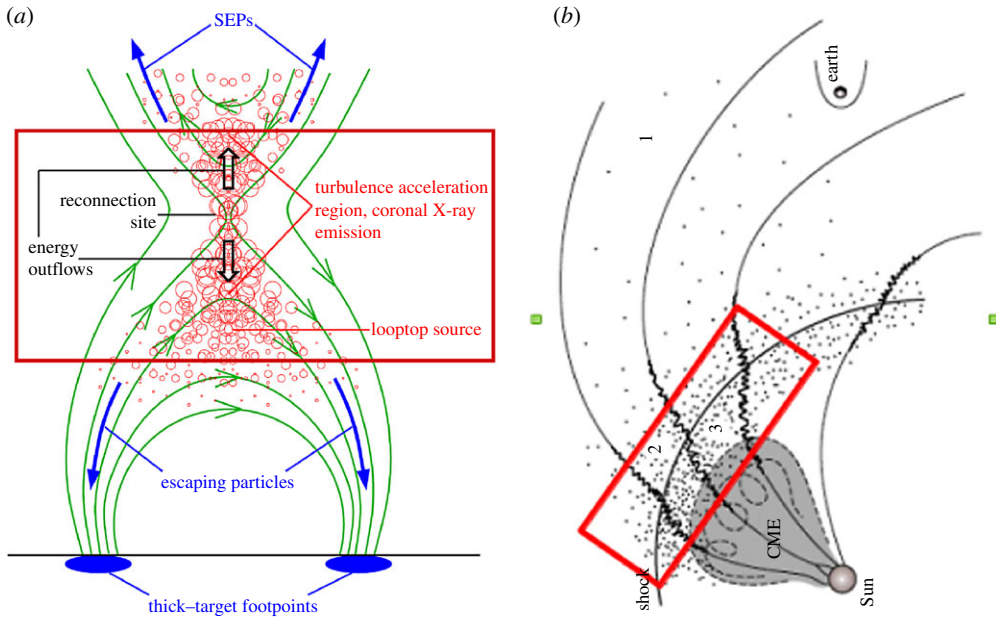
Figure 1. (*a*) Schematic of the reconnecting field (solid green) forming closed coronal loops and open field lines, presumably extending higher up into the corona and the solar wind. The red foam represents turbulence. Acceleration probably takes place in the outflow regions above and below the X-point. Particles (temporarily) trapped here produce the radiation seen above the closed loops, and particles escaping these regions up and down (blue arrows) are observed at 1 AU as SEPs and produce the non-thermal radiation (mainly at the two footpoints; blue ovals), respectively. (*b*) Similar schematic view, joining the flare site field lines to the CME, the shock, and beyond (from Lee [3]). The rectangles define the boundary of the acceleration sites and represent the leaky box [4]. (Online version in colour.)

2. Key observational constraints for particle acceleration theories in the solar corona

(a) Location of solar energetic particles acceleration and release sites

The detection of a SEP event at any given location in the heliosphere requires a direct magnetic connection to the region where the particle acceleration and release takes place. When the accelerated charged particles are released into open magnetic field lines, they propagate from their production site through the interplanetary medium, spiralling along the field lines until their detection through instruments that perform *in situ* measurements. Since particles tend to move more easily along the magnetic field lines than across, the relative location of the parent active region (AR) with respect to the location of the observing point is considered to be an important parameter for the detection of an SEP event.

Eruptions that take place at ARs with western locations on the solar disk seem to be more likely to record a SEP event, due to the Parker spiral shape of the interplanetary magnetic field [15]. This picture is mostly consistent with the impulsive-flare-related SEP events being associated with localized sources close to the Sun. Gradual-CME-related SEP events are usually detected at widely separated locations in the heliosphere [16,17]. Remote-sensing observations and *in situ* measurements from multiple vantage points (SoHO, STEREO, ACE and Wind) have significantly improved our knowledge about the large longitudinal spread of SEP events and also helped to define the locations of the possible particle acceleration and release sites. Widespread (i.e. greater than 90–180°) and usually long duration (i.e. greater than 2 h) SEP events (gradual-CME-related SEPs), are associated with the spatial and temporal evolution of coronal and interplanetary

shock waves that are presumably driven by fast and wide CMEs. Additionally, multi-spacecraft observations have challenged in some cases the expectation of a narrow longitudinal distribution of impulsive SEP events. The analysis of Wiedenbeck *et al.* [18] showed that impulsive events can also be detected over wide longitudinal ranges.

A combination of several datasets, including remote-sensing and *in situ* observations, made it possible to relate the different aspects of the eruptive events to the SEP events seen at 1 AU. For the gradual-CME-related SEP events, the CME-driven shock waves are considered to have an important role in the acceleration and the release of SEPs over a wide range of longitudes. Rouillard *et al.* [19], by using multi-viewpoint observations of the CME and the solar corona for an eruptive event that occurred on 21 March 2011, showed that the CME extension over a wide longitudinal range in the corona was responsible for the large longitudinal spread of a SEP event. A long list of continued studies signified even further the role of the expanding shock waves [20–24] or EUV waves [25–28] in the longitudinal spread of SEP events as observed at distant magnetically connected s/c. In any case, there is a converging argument that the acceleration process itself occurs over a wide range of longitudes rather than in a small source region, where the accelerated particles could be transported before being injected at distant longitudes.

(b) Critical properties of coronal mass ejections and the associated shock waves

A series of studies have shown a significant correlation of SEP peak intensities with the speed and other properties of the associated CMEs [7,29–34]. Kahler *et al.* [30] showed that the speed of the CMEs associated with SEPs have a good correlation with the energetic proton peak intensities, and additionally Kahler *et al.* [32] found that the total CME energy is well correlated with either the SEP peak intensities or the total SEPs energy. Furthermore, Richardson *et al.* [33] compared the estimates of CME parameters using several catalogues to reduce the projection effects for the correlations with the proton intensities. They found that the CME speed in quadrature when compared with the SEPs peak intensity results in higher correlations.

The comparisons between critical parameters of CMEs and SEP properties have revealed significant correlations, however, in any case, there is a large spread (approx. 3 decades) in the SEP properties for a given CME parameter. One of the important factors for the large spread in the correlations may arise from the use of CME parameters as a proxy for the CME-driven shock wave characteristics. In addition, the involved uncertainties in determining the CME speed and other parameters, while they are projected measures in the plane of the sky, may also be an important factor. Nevertheless, the CME parameters, such as their speed and width, can be easily inferred from remote-sensing observations and serve as a rather good basis for the current SEP forecasting schemes [16].

The role of shock waves in energetic particle acceleration and release has been further elucidated thanks to the constantly evolving techniques that have been developed, making it possible to infer shock parameters from remote-sensing observations. Those techniques integrate the observations provided by instruments located at multiple viewpoints. The density compression ratio and Alfvénic Mach number are some of the critical shock parameters that can be deduced from remote-sensing observations [24,35–37]. Kwon *et al.* [24] showed that there is a wide spatial range where the shock waves, analysed in their study, are super-critical for a long duration with an average density compression ratio of 2.1–2.6. This result provides additional support to the expectation of previous studies that the wide extent of these shocks is the reason for the distribution of SEPs over a very wide range of heliospheric longitudes.

Additionally, MHD shock modelling [38,39] or a combination of shock forward modelling with parameters of the background corona from MHD simulations [40], seem to be essential to determine the shock wave properties at the apparent acceleration/release sites of SEPs. The studies of Kozarev *et al.* [38,39] and Rouillard *et al.* [40] suggest a link between the shock characteristics and the SEPs measured *in situ* (see also [41]). Additionally, Kouloumvakos *et al.* [42], from an extensive comparison between the three-dimensional (3D) shock parameters at the magnetically well-connected regions and the SEPs characteristics, showed significant

correlations, better than those with the CME properties. The best correlation is established for the comparison between the shock Alfvénic Mach number and the SEPs peak intensity greater than 70%. Additionally, Kouloumvakos *et al.* [42] showed that the evolution of the shock parameters at the well-connected regions can sufficiently explain the characteristics of the observed SEP events even for the far connected cases. These results signify further the role of the shock waves in particle acceleration and additionally seem to establish a very good association between the longitudinal extent of the SEP event in the heliosphere and that of the lateral extension of the CME and the CME-driven shock wave.

## (c) Impulsive, gradual and mixed events

The dichotomous picture of SEP events has proven to be useful; however, both flares and CMEs are associated with almost all kind of SEP events, so it is often difficult to distinguish the particle accelerator unambiguously. Additionally, there are SEPs with properties that fail to strictly follow the dichotomous picture [43]. This indicates that the classical picture might be a simplification and a third category of events could exist [34]. This third category, so-called *hybrid or mix events*, have SEP properties that resemble gradual SEP events, but also demonstrate properties of impulsive SEPs. In this category, the SEP events may result from both solar flare or CME-driven shock acceleration. In this context, the acceleration mechanism should be a combination of stochastic acceleration and shock drift acceleration in different timescales of the SEP evolution.

The difficulty of making a dichotomous separation of SEP events is also reflected in studies that examine the association between type III, II and IV radio bursts and SEP events. Radio emissions have a rich diagnostic potential about the acceleration and propagation of SEP as well as shocks. Miteva *et al.* [44] showed that SEP events, either gradual or impulsive, were found to have the highest association rate with type III radio bursts and a lower association with type II bursts. Additionally, Kouloumvakos *et al.* [45] examined the association of the SEP release time, as inferred by the velocity dispersion analysis, with transient solar radio emissions to identify the most relevant acceleration processes. Their study showed that both flare- and shock-related particle release processes are observed in major proton events at greater than 50 MeV and a clear-cut distinction between flare-related and CME-related SEP events is difficult to establish. The proton release was found to be most often accompanied by both type III and II radio bursts, but a good association rate only with type III radio bursts was also found.

(d) Elemental abundance and spectral variability

The abundance of elements and isotopes of SEPs have been extensively used as indicators of their acceleration and transport and also served as the earliest indication of the dichotomous picture of SEPs [46]. Gradual events are in general considered to have a composition similar to that of the corona or solar wind (SW), while impulsive events typically have enhanced element and isotope ratios.

The SEPs energy spectra and their variability is another important characteristic that provides useful information about the acceleration processes involved. From an analysis of 16 ground level enhancements (GLE), Mewaldt *et al.* [47] found that the energetic proton spectra exhibited breaks between approximately 2 and 50 MeV and that they were better represented by a double power-law function (figure 2). This study also showed that GLE spectra are harder, with spectral indices $\gamma \sim 3$ above 40 MeV/nucleon, in comparison with other SEP events. Evidence of spectral hardening might suggest that a different or a more complex acceleration process could dominate at higher energies [16]. Additionally, Mewaldt *et al.* [48] showed that for some large multi-spacecraft SEP events there is a wide divergence in spectral slopes for the same event. The energy spectrum of the SEPs that were observed by the best-connected spacecraft to the source region exhibits an energy spectrum above the spectral break as hard or harder than the others, with the exception of the 3 November 2011 event. The spectral differences may be attributed
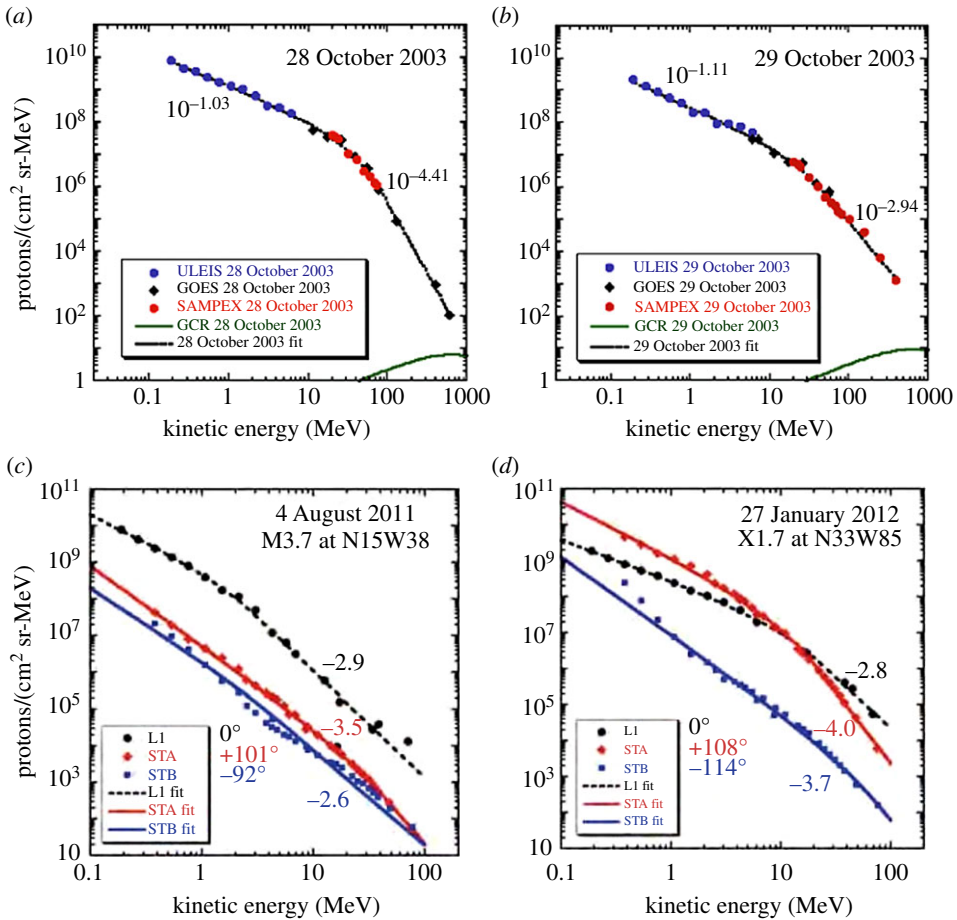
Figure 2. (*a,b*) Proton fluence spectra for two GLE events from Mewaldt *et al.* [47]. (*c,d*) Proton fluence spectra from multi-spacecraft observations (STA, STB and near-Earth) for two large SEP events, from Mewaldt *et al.* [48]. (*c*, 4 August 2011; *d*, 27 January 2012). The measured spectra are fitted with a double power-law function. (Online version in colour.)

to different shock geometry, the relative contribution of shock acceleration and downstream turbulent reconnection [49–52], or the acceleration in the current fragmentation of the eruptive large-scale magnetic structures.

(e) What about solar energetic particles without flares or coronal mass ejections?

Flares and CMEs are the two main manifestations of solar eruptions and typically they accompany each other. However, a significant fraction of intense flares seem not to be accompanied by CMEs [53]. Those cases have been termed as confined flares since they are unaccompanied by any ejection signature. Some of those confined events were additionally lacking any SEP signature, even those that were located at the western solar hemisphere [54]. Klein *et al.* [55] concluded that a possible reason why major solar flares in the western hemisphere are not associated with SEPs is the confinement of particles accelerated in the impulsive phase. On the other hand, only a few SEP events are associated with a CME and no flare signatures in the corona. An old paradigm is an event presented in Kahler *et al.* [56], which included a filament eruption and a CME without an impulsive flare or radio emission in the low corona, and it was associated with a SEP event.

(f) A summary of the key observational points

A complete theory of the coronal sources of the SEP is currently absent since many key observations are still missing. A few important points discussed in this section are:

— The impulsive-flare-related SEP events are associated with localized sources close to the Sun. Gradual-CME-related SEP events are usually determined at widely separated locations in the heliosphere.
— SEP events with characteristics resembling impulsive events can also be detected over wide longitudinal ranges.
— The simplistic dichotomy of the SEP events in impulsive and gradual is not present in all SEP events.
— Observations are consistent with the acceleration process occurring over a wide range of longitudes rather a small source region, and the accelerated particles could be transported before being injected at distant longitudes.
— The comparison between CME or shock parameters and SEP properties shows significant correlations, better than the correlations with flare parameters.
— SEP events, either gradual or impulsive, were found to have high association with both type III and type II radio bursts.
— Gradual events are generally considered to have a composition similar to that of the corona or the SW, while impulsive events typically have enhanced element and isotope ratios.
— The energy spectra based on the GLE show a double power law, with the break between 2 and 50 MeV.
— Observations have revealed that most of the SEP events are associated with both flares and CMEs. Several intense flares that seem not to be accompanied by a CME also were lacking SEPs.

We will discuss in §7 how the key observational points listed above can be interpreted by the acceleration mechanisms presented in this review.

3. The evolution of magnetic topologies and eruptive phenomena

Solar ARs, coronal holes and the quiet sun are all driven by the turbulent photospheric flows and the emergence of new magnetic flux (see Archontis & Syntelis [13]).

The acceleration mechanisms for SEP are closely related with the evolution of the 3D eruptive magnetic topologies and the energy release processes [46]. The magnetic eruptions relate all the known particle acceleration mechanisms (strong turbulence and CME-related shocks). In figure 3, a sketch of the magnetic field topologies closely related with the observed properties of SEP events is presented. It is important to connect the sketch in figure 3 with the evolution of eruptive magnetic topologies driven by turbulent photospheric motions [14]. In the following, we present examples of eruptive magnetic topologies using as initial topology nonlinear force-free extrapolations of observed magnetograms, as driven by photospheric motions [57–59].

Inoue *et al.* [58] performed an MHD simulation in order to reveal the 3D dynamics of the magnetic fields associated with an X9.3 solar flare. They first performed an extrapolation of the 3D magnetic field based on the observed photospheric magnetic field prior to the flare and then used this as the initial condition for the MHD simulation, which revealed a dramatic eruption (figure 4). In particular, they found that a large coherent flux rope composed of highly twisted magnetic field lines formed during the eruption. A series of small flux ropes were found to lie along a magnetic polarity inversion line prior to the flare. Reconnection occurring between each flux rope during the early stages of the eruption formed the large, highly twisted flux rope. Furthermore, they observed a writhing motion of the erupting flux rope. Understanding these dynamics is of high significance in order to increase the accuracy of space weather forecasting. Inoue *et al.* [58] reported on the detailed dynamics of the 3D eruptive flux rope and discussed the
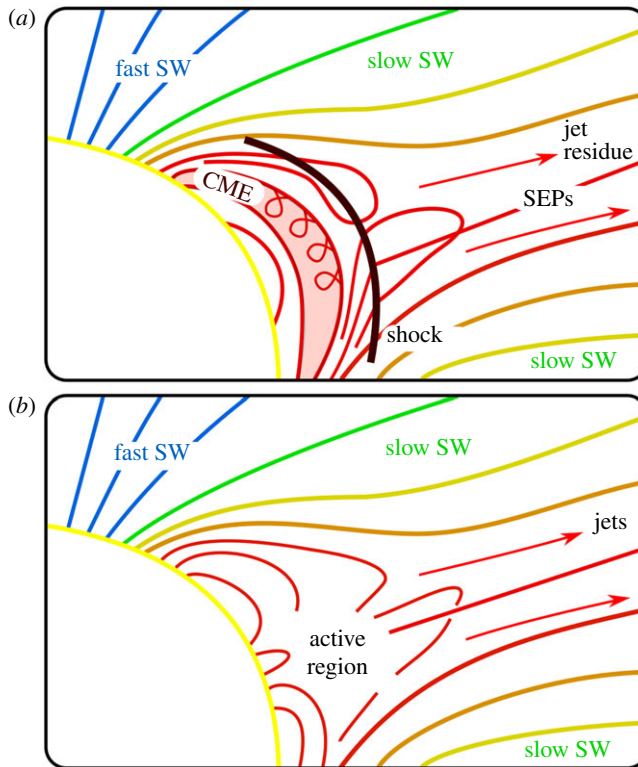
Figure 3. Sketch of possible sources of SEPs. (*a*) A CME-driven shock wave (grey) that accelerates plasma from the high corona, and residues from jets. Blue field lines track the fast solar wind (SW) from coronal holes that have photospheric sources similar to the slow SW, but less trapping and divergence. (*b*) An active region (red), containing closed loops from which solar jets emerge. Field lines carrying the slow SW (yellow and green) diverge from open field lines from the photosphere outside of active regions [46].

possible mechanisms of the writhing motion. The brief presence of a large-scale current sheet is apparent but soon after it fragments, it forms a turbulent environment in the same location.

In figure 5, 3D simulations of a data-driven eruption or flux emergence, interacting with the ambient magnetic field and forming a blow out jet, are shown [59]. The MHD model of Jiang *et al.* [59] was initialized with a potential field extrapolation of the vertical component of the photospheric field, and a highly tenuous plasma in hydrostatic, isothermal state (with solar gravity) was assumed to approximate the coronal low-β plasma condition. They drive the model continuously by supplying the bottom boundary with a data stream of photospheric vector magnetograms. The Heliospheric Magnetic Imager (HMI) provides routinely high-quality vector magnetograph data at the photosphere with spatial resolution of 1 arcsec and cadence of 12 m, which is adequate for tracking the relatively long-term (hours to days) evolution of AR magnetic structures from their formation to eruption. To ensure that the input of boundary vector fields is self-consistent, they use the method of projected characteristics, which has its foundation in the wave-decomposition principle of the full MHD system. It has been shown that such a method can naturally simulate the transport of magnetic energy and helicity to the corona from below.

In the simulations reported above, the spontaneous formation of reconnecting current sheets at several locations in the evolving structures is apparent. On the other hand, formed large-scale reconnecting current sheets are also fragmented and disappear rapidly, forming a turbulent reconnecting environment [6,60,61]. In realistic magnetic topologies, being led to eruption through photospheric turbulent flows or the emergence of new magnetic flux, distributed reconnecting current sheets and large amplitude magnetic disturbances will always be present.
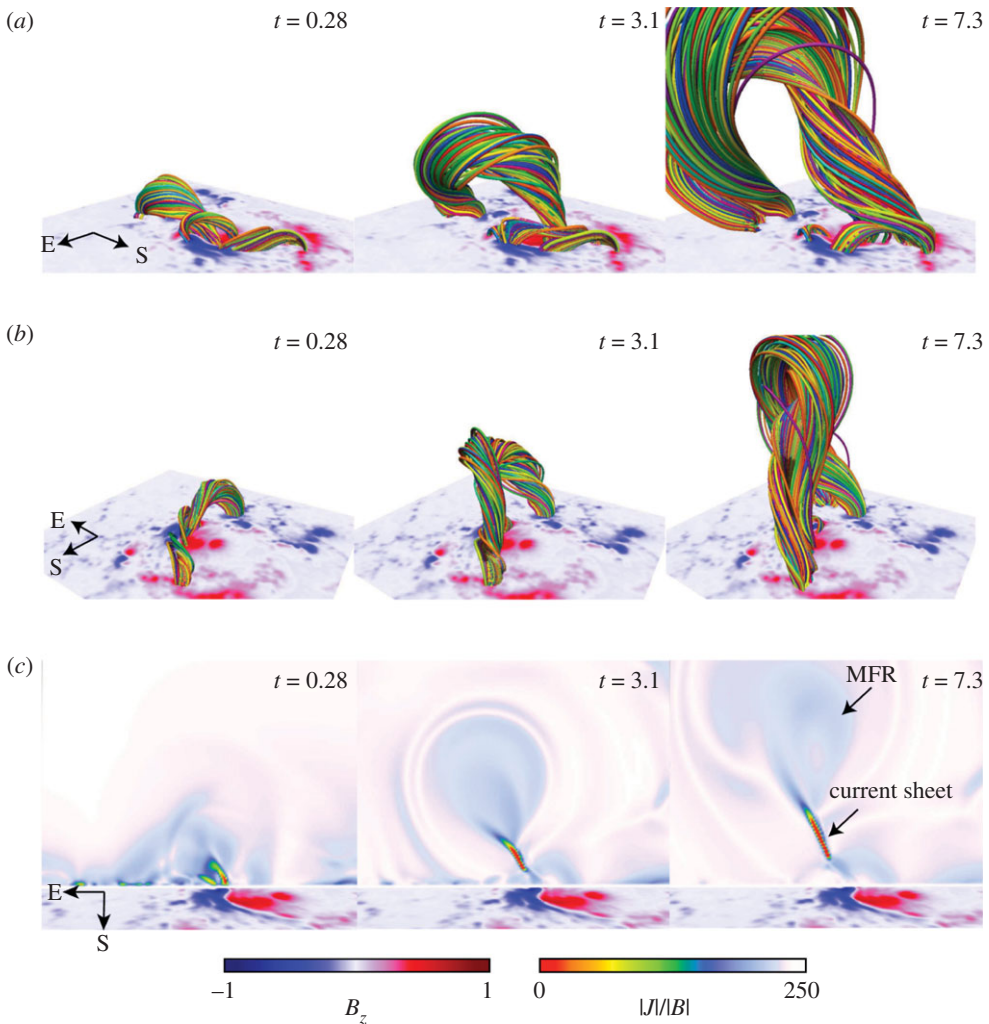
Figure 4. Temporal evolution of the formation and dynamics of an eruptive magnetic flux rope (MFR). (*a*,*b*) The field lines from different viewing angles. E and S stand for east and south. An animation of these panels is available in the original article, its duration is 4 s. (*c*) Temporal evolution of $|J|/|B|$ plotted in the $x-z$ plane at $y = 0.38$, with a viewpoint from the south [58].

This is in contrast to the static 2D cartoon (figure 1) used extensively in the current literature and referred to as the 'standard' flare model, where the monolithic current sheet is artificially maintained for long times and its jets generate weak turbulence [4].

Numerous articles that provide examples of MHD simulations of erupting flux ropes leading to the formation of current sheets have been reported in the past. These models initiate the simulations with an artificial magnetic loop stressed by simple photospheric motions. The main goal of these simulations was to reproduce the standard flare model shown in figure 1.

4. Energization of particles in weak and strong turbulence during explosive events

(a) Weak turbulence

In the astrophysics community, the term 'turbulence' is synonymous to 'weak turbulence' and refers to stochastic interaction of particles with low amplitude ($\delta B/B \ll 1$) linear MHD waves [8,62]. The stochastic (or second order) acceleration of particles was first proposed and analysed
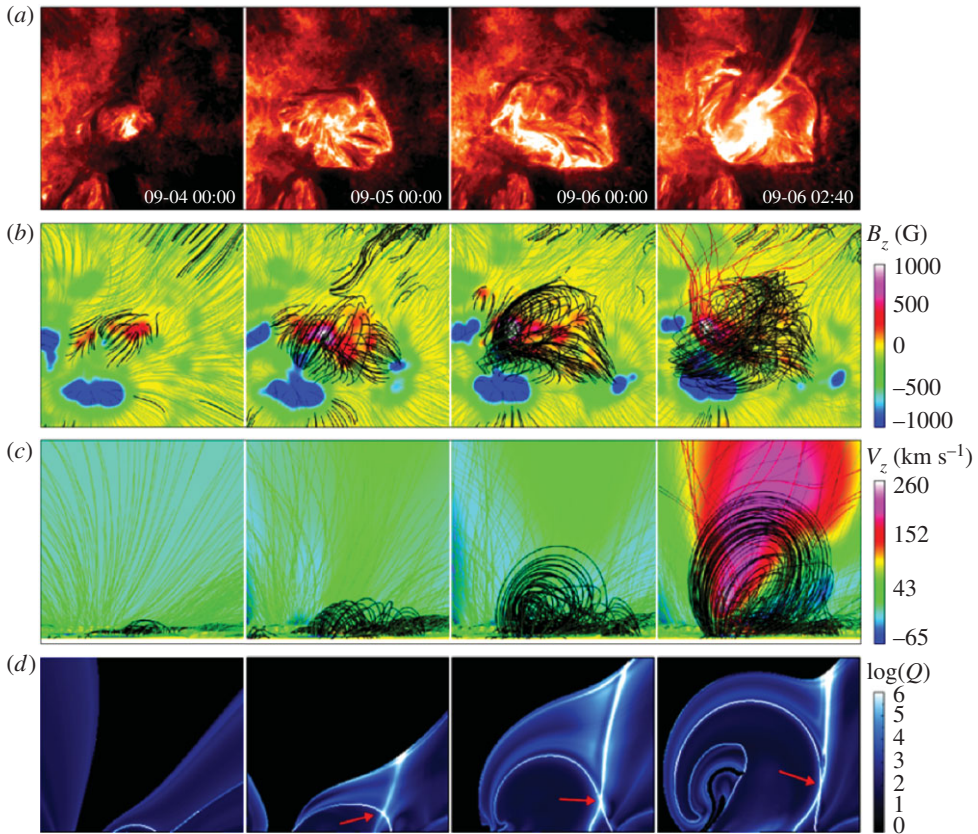
Figure 5. (*a*) Images at different times from the initial emergence to the eruption. (*b*) Top view of the corresponding magnetic field evolution at different times ($t = 0, 12, 24, 48$ and 57) from the MHD model. The field lines are traced from footpoints evenly distributed at the bottom surface, which is shown with the photospheric magnetic flux map. Field lines closed (open) in the box are coloured black (green), while those becoming open from closed during the eruption are coloured red. (*c*) Side view of the magnetic field lines from south (i.e. the horizontal and vertical axes are x and z, respectively). The background shows a 2D central cross-section of the 3D volume and its colour indicates the value of the vertical component of the velocity. (*d*) Vertical cross-sections of the evolving magnetic topology show the spontaneous formation of a large-scale current sheet [59].

by Fermi [63] as a mechanism for the acceleration of Cosmic Rays [64]. The core of his idea had a larger impact on nonlinear processes in general and has been the driving force behind all subsequent theories on charged particle energization in space and astrophysical plasmas. In the original treatment, relativistic particles were accelerated by collisions with very massive, slowly moving magnetic clouds (scattering centres). The rate of the systematic energy gain of the charged particles with the scatterers is proportional to the square of the ratio of the magnetic cloud speed (V) to the speed of light (c), i.e. $(V/c)^2$. A few years after the initial article by Fermi, Davis [65] and Parker & Tidman [66] emphasized the stochastic nature of the initial Fermi proposal and they estimated analytically the transport coefficients, using an idealized assumption for the interaction of the scatterers with the particles. Parker & Tidman [66] assumed that the scattering centres are randomly moving and applied their model to solar flares, accelerating protons from the thermal distribution.

The initial idea put forward by Fermi was soon replaced in the astrophysical literature with a new suggestion based on the interaction of charged particles with a Kolmogorov spectrum of low-amplitude MHD waves ($\delta B/B \ll 1$), and the acceleration process was renamed as stochastic (weak) turbulent heating and acceleration or simply stochastic acceleration by turbulence ([65,

67,68]; see also the reviews by Miller & Petrosian [5,8]). When the amplitude of the waves (δB) is much smaller than the mean magnetic field B, the transport coefficients are estimated with the use of the quasi-linear approximation, and by solving the transport equations one can estimate the evolution of the energy distribution of the particles [69,70]. The Fokker–Planck equation became the main tool for the analysis of the evolution of energy distributions of particles. The diffusion (Fokker–Planck) equation estimates the rate of change of the energy distribution $n(W, t)$ of the accelerated particles. In order to simplify the diffusion equation, spatial diffusion was dropped, since it was assumed that it is not important inside the acceleration region,

$$\frac{\partial n}{\partial t} + \frac{\partial}{\partial W}\left[Fn - \frac{\partial(Dn)}{\partial W}\right] = -\frac{n}{t_{esc}} + Q, \tag{4.1}$$

where t_{esc} is the escape time from an acceleration volume with characteristic length L, Q is the injection rate, F and D are the transport coefficients. The escape time is also kept as a free parameter in most applications of stochastic acceleration.

The main disadvantage of the stochastic acceleration of particles through low-amplitude MHD linear waves is the fact that nobody so far has proved that there is a link with the well-known energy release processes during explosive solar events (e.g. magnetic reconnection in the spontaneously formed current sheets). Petrosian [4] and others used the cartoon of the 'standard' flare model (figure 1) to link the reconnecting current sheet with the weak turbulence needed to accelerate the particles. As we will see below, fully developed turbulence will naturally provide a link between energy release processes and particle acceleration during impulsive events.

(b) Strong turbulence

The highly twisted magnetic topologies born out from the current simulations mentioned in the previous section, lead to a different regime of turbulence with remarkably more complex mixing of unstable current sheets and large amplitude magnetic disturbances; this state of turbulence is also called 'turbulent reconnection' (see the recent review [71] and references therein).

We use the term 'turbulent reconnection' to define an environment where large-scale magnetic discontinuities with $\delta B/B > 1$ coexist with randomly distributed unstable current sheets (UCS) [72,73]. The importance of turbulent reconnection in many space and astrophysical systems has been discussed in detail in many recent reviews [74,75].

Isliker *et al.* [76] consider a strongly turbulent environment as it naturally results from the nonlinear evolution of the MHD equations, in a similar approach as in Dmitruk *et al.* [77]. Thus, they did not set up a specific geometry of a reconnection environment or prescribe a collection of waves [78] as turbulence model, but allow the MHD equations themselves to build naturally correlated field structures (which are turbulent, not random) and coherent regions of intense current densities (current filaments or CS).

The 3D, resistive, compressible and normalized MHD equations used are

$$\partial_t \rho = -\nabla \cdot \mathbf{p} \tag{4.2}$$

$$\partial_t \mathbf{p} = -\nabla \cdot (\mathbf{pu} - \mathbf{BB}) - \nabla P - \nabla B^2/2 \tag{4.3}$$

$$\partial_t \mathbf{B} = -\nabla \times \mathbf{E} \tag{4.4}$$

$$\partial_t (S\rho) = -\nabla \cdot [S\rho\mathbf{u}] \tag{4.5}$$

with ρ the density, $\mathbf{p}$ the momentum density, $\mathbf{u} = \mathbf{p}/\rho$, P the thermal pressure, $\mathbf{B}$ the magnetic field,

$$\mathbf{E} = -\mathbf{u} \times \mathbf{B} + \eta \mathbf{J} \tag{4.6}$$

the electric field, $\mathbf{J} = \nabla \times \mathbf{B}$ the current density, η the resistivity, $S = P/\rho^\Gamma$ the entropy and $\Gamma = 5/3$ the adiabatic index.

Isliker *et al.* [76] solved the 3D MHD equations numerically (with the pseudo-spectral method [79], combined with the strong-stability-preserving Runge–Kutta scheme [80]) in Cartesian
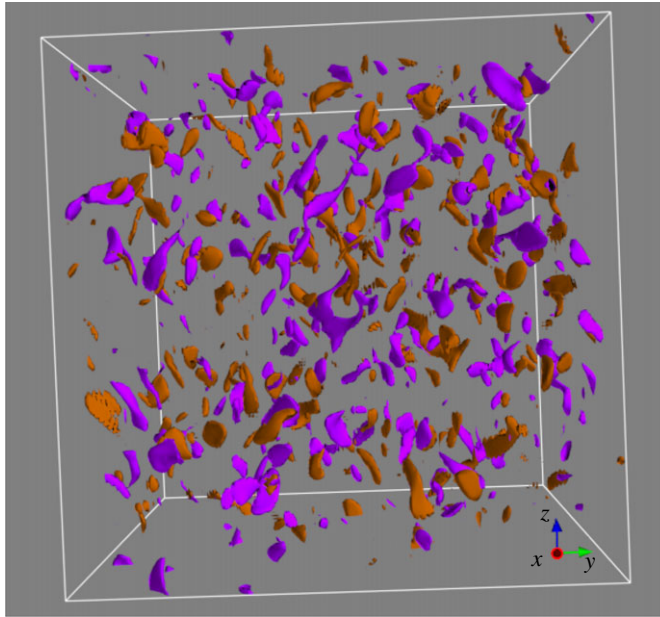
Figure 6. Iso-contours of the supercritical current density component J_z (positive in brown negative in violet) [76].

coordinates and by applying periodic boundary conditions to a grid of size $128 \times 128 \times 128$. As initial conditions, they use a fluctuating magnetic field $\mathbf{b}$ that consists of a superposition of Alfvén waves, with a Kolmogorov-type spectrum in Fourier space, together with a constant background magnetic field $\mathbf{B}_0$ in the z-direction, so the total magnetic field is $\mathbf{B} = \mathbf{B}_0 + \mathbf{b}(x, y, z, t)$. The mean value of the initial magnetic perturbation is $< b > = 0.6B_0$, its standard deviation is $0.3B_0$, and the maximum equals $2B_0$, so that they indeed consider strong turbulence. The initial velocity field is 0, and the initial pressure and energy are constant.

The structure of the z-component of the current density J_z is shown in figure 6. For the MHD turbulent environment to build, Isliker *et al.* [76] let the MHD equations evolve until the largest velocity component starts to exceed twice the Alfèn speed. The magnetic Reynolds number at final time is $< |\mathbf{u}| > l/\eta = 3.5 \times 10^3$, with $l \approx 0.01$ a typical eddy size. The overall picture in figure 6 demonstrates the spontaneous formation of current sheets. This result resembles the 2D simulations of Biskamp & Walter [81] almost 30 years ago. Similar results were obtained by Arzner *et al.* [78,82], using Gaussian fields or the large eddy simulation scheme.

The statistical properties of the current sheets formed inside strongly turbulent environments have been analysed in depth in 2D and 3D simulations by many researchers [83–87]. Zhdankin *et al.* [87] developed a framework for studying the statistical properties of current sheets formed inside a magnetized plasma using a 3D reduced MHD code. The current fragmentation in an x-y-plane, which includes current sheets, is shown in figure 7. They were able to show that a large number of current sheets do not contain reconnection sites, and likewise, many reconnection sites do not reside inside current sheets. The most striking characteristic of the current sheets formed spontaneously inside the strongly turbulent plasma is the probability distribution of the dissipated energy $\varepsilon = \int \eta j^2 \, dV$, which follows a power law in shape, as reported by Zhdankin *et al.* [87] (figure 7).

Ambrosiano *et al.* [88] were the first to analyse the evolution of test particles inside turbulent reconnection modelled by the simulations of Matthaeus & Lamkin [72]. Many years later several researchers returned to this problem and followed the evolution of a distribution of particles inside a snapshot of the 3D evolution of a spectrum of MHD waves [77,82,89]. Isliker *et al.* [76] use the simulations already reported to explore the evolution of test particles inside a
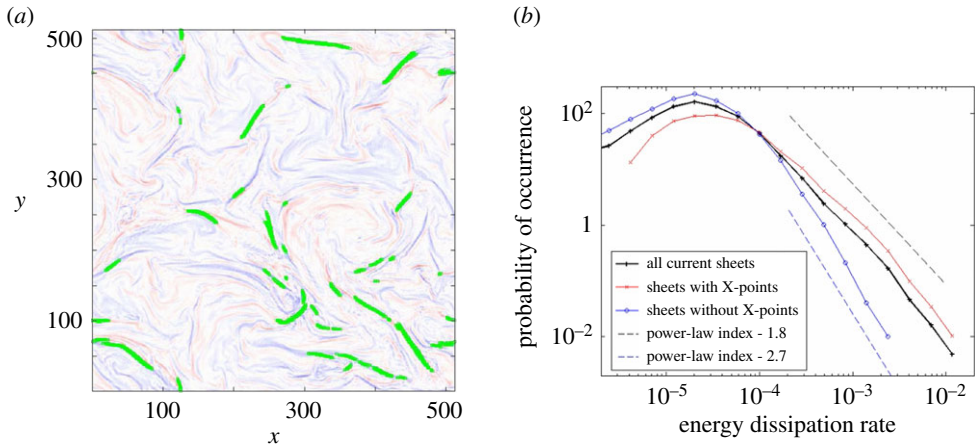
Figure 7. (*a*) Current density in an *x*-*y*-plane cross-section of data. Red indicates negative current and blue indicates positive current. Identified current sheets in the plane are marked by green colour. (*b*) Probability distribution of the current sheet Ohmic dissipation rate. The distribution from all current sheets (black) shows a power-law tail with index near −1.8 (from [87]).

large-scale, non-periodic, turbulent reconnection environment. The test-particles are tracked in a fixed snapshot of the MHD evolution, and they evolve the particles for short times, so they do not probe the scattering of particles off waves, but the interaction with electric fields. In this particular numerical experiment, anomalous resistivity effects were taken into account. Physical units are introduced by using the parameters $L = 10^5$ m for the box-size, $v_A = 2 \times 10^6$ m s^{-1} for the Alfvén speed and $B_0 = 0.01$ T for the background magnetic field. Isliker *et al.* apply a cubic interpolation of the fields at the grid-points to the actual particle positions. The relativistic guiding centre equations (without collisions) are used for the evolution of the position **r** and the parallel component $u_{||}$ of the relativistic 4-velocity of the particles. The test-particles they consider throughout are electrons. Initially, all particles are located at random positions, they obey a Maxwellian distribution $n(W, t = 0)$ with temperature $T = 100$ eV. The simulation box is open, the particles can escape from it when they reach any of its boundaries.

The acceleration process is very efficient, and they consider a final time of 0.002 s (7×10^5 gyration periods), at which the asymptotic state has already been reached. Figures 6 and 8*a* show the component J_z in the regions of above-critical current density, which clearly are fragmented into a large number of small-scale current filaments (current-sheets) that represent coherent structures within the nonlinear, super-Alfvénic MHD environment. The figure also shows the orbits of some energetic particles. The particles can lose energy, yet they mostly gain energy in a number of sudden jumps in energy (see also figure 8*b*), the energization process thus is localized and there is multiple energization at different current filaments. Figure 8*c* shows the energy distribution at final time, which exhibits a clear power law part in the intermediate to high energy range with power-law index −1.51, with a slight turnover at the highest energies. There is also moderate heating, and the initial temperature has roughly been doubled (qualitatively similar characteristics of the acceleration process have been observed in [78] and in the PIC simulations of [61,90]).

As shown in [76], the distribution of energy increments exhibits a power-law tail, which implies that the particle dynamics is anomalous, with occasionally large energy steps being made; the particles perform Levy-flights in energy space when their dynamic is interpreted as a random walk. Isliker *et al.* [76] introduced a formalism for a fractional transport equation (FTE) that is able to cope with this kind of non-classical dynamics. The solution of the FTE at final time is also shown in figure 8*c*, obviously the FTE reproduces very well the power-law tail in its entire extent, which confirms that transport in energy space is of a fractional nature.
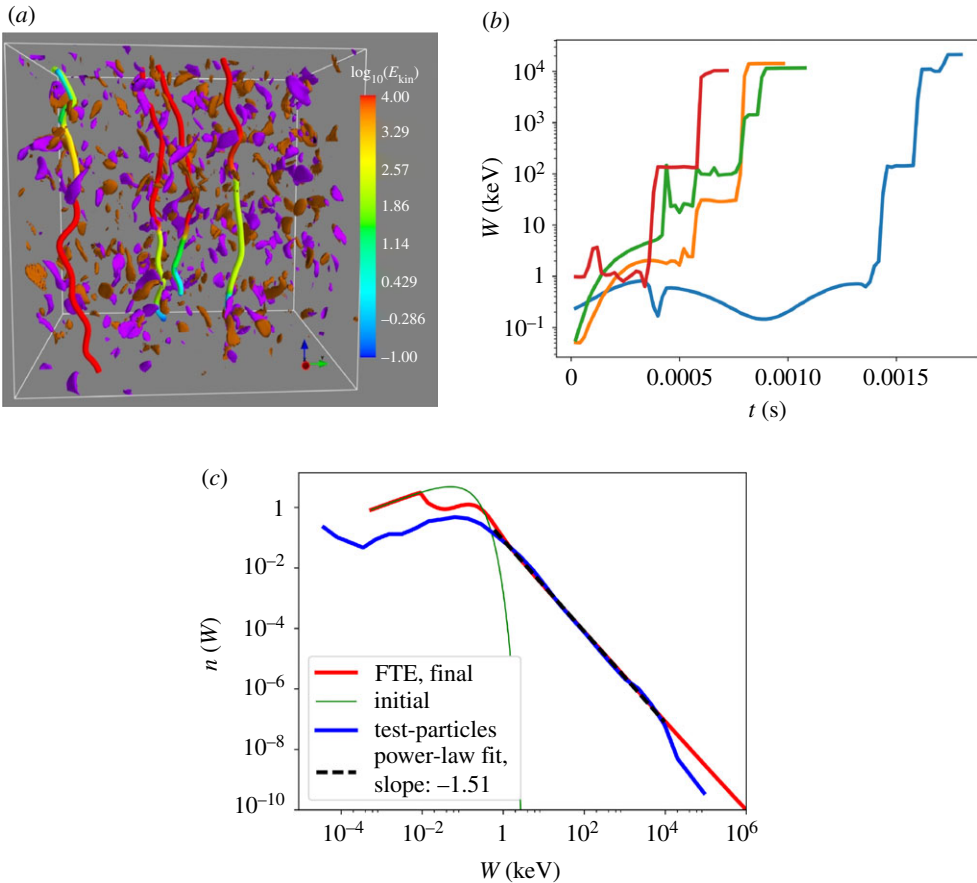
Figure 8. (*a*) Particle orbits inside the simulation box, coloured according to their kinetic energy (*b*) Typical particle trajectories in energy of some accelerated particles. (*c*) Initial and final (at $t = 0.002$ s) kinetic energy distribution from the test-particle simulations, together with a power-law fit, and the solution of the fractional transport equation (FTE) at final time [76].

Pisokas *et al.* [91] analysed the stochastic Fermi acceleration of ions and electrons interacting with large-scale magnetic fluctuations using a simple model, illustrated in figure 9*a*. A 3D grid with linear size L is used, and it is assumed that a small percentage of the grid points are active (magnetic disturbances) and the rest are passive. Ions interacting with active grid points gain or lose energy stochastically, following the initial suggestion by Fermi [63]. The asymptotic energy distribution of the accelerated ions is shown in figure 9*b* for parameters similar to the ones in the low corona.

In turbulent reconnection, stochastic scattering at large-scale disturbances coexists with acceleration at UCSs. It is natural to ask how the ambient particles react if the two Fermi accelerators act simultaneously. Pisokas *et al.* [92] discuss the synergy of the energization at large-scale magnetic disturbances (stochastic scatterers) with the systematic acceleration by UCSs.

5. Energization of particles during magnetic flux emergence

In §3, we discussed the MHD evolution of data-driven large-scale magnetic eruptions. One of the important results was the spontaneous formations of current sheets of different scales at different locations inside the evolving magnetic topology. The evolution of the large-scale current sheets and their role in reorganizing the magnetic topology and accelerating particles was not discussed in §3, since all these physical processes are below the resolution of the large-scale simulations. In this section, we consider higher resolution MHD simulations of emerging magnetic flux
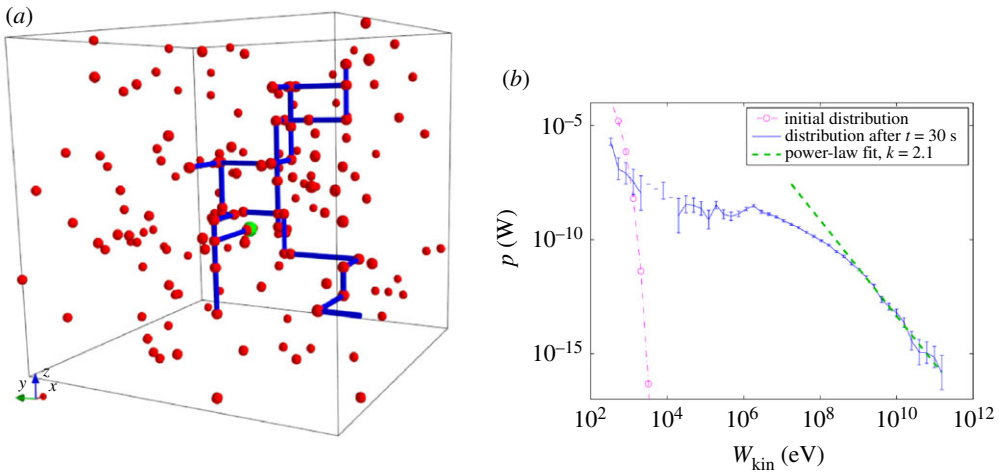
Figure 9. (a) The trajectory of a typical particle (blue tube) inside a grid with linear dimension L. Active points are marked by spheres in red colour. The particle starts at a random grid-point (green sphere), moves along a straight path on the grid till it meets an active point and then it moves into a new random direction, and so on, until it exits the simulation box. (b) Energy distribution of the ions at $t = 0$ s and $t = 30$ s (stabilized) [91].

interacting with the ambient magnetic field and forming a large-scale current sheet that fragments and becomes an efficient particle accelerator.

Emerging magnetic flux into preexisting magnetic fields drives the formation of large-scale reconnecting current sheets in tens of minutes and can be the source of several eruptive phenomena, e.g. flares, prominence eruptions, jets, CMEs [93,94,94–105]. The emerging flux will drive a standard or a blowout jet, which can be the source of impulsive or gradual SEP events (see the recent review in [103]).

Arhontis & Hood [99] use a 3D resistive MHD code to follow the emergence of new magnetic flux into the preexisting magnetic field in the corona. The formation and subsequent fragmentation of the large-scale reconnecting current sheets is obvious in their numerical study (figure 10). Details of their simulation and their results can be found in their article.

Isliker et al. [106] use the results from the numerical simulations of Archontis & Hood [99] but focus on the statistical properties of the electric fields and the energy transport of electrons in the vicinity of the fragmented large-scale current sheet (figure 11). They first consider the energization of particles at the standard jet, snapshot 30. Electrons are considered as test-particles, the standard integration time is 0.1 s, and 100 000 particles are traced in any case by using the relativistic guiding centre approximation to the equations of motion. The initial spatial position is uniform random in the region around the main reconnection region, as out-lined by the green cube in figure 11. The initial velocity is random with Maxwellian distribution (i.e. Gaussian distribution of the velocity components), with temperature $\approx 9 \times 10^5$ K. For each simulation, a set of 100 monitoring times has been predefined, including the final time, at which the velocities and positions of the particles are monitored for the purpose of a statistical analysis to be done at equal times for all the particles. Separate track is kept of the particles that leave before the final time.

Figure 12 shows the distribution of the kinetic energies of the particles after 0.1 s, together with the initial distribution and the distribution of the leaving particles (as collected at the times the individual particles leave). The final energy distribution is of Maxwellian shape at the low energies, and exhibits a slightly modulated power-law tail. The maximum energy reached is about 1 MeV, and a power-law fit to the tail of the kinetic energy distribution yields an index of about −1.87. 13% of the 100 000 particles that are traced have left after 0.1 s, and they have energies in the
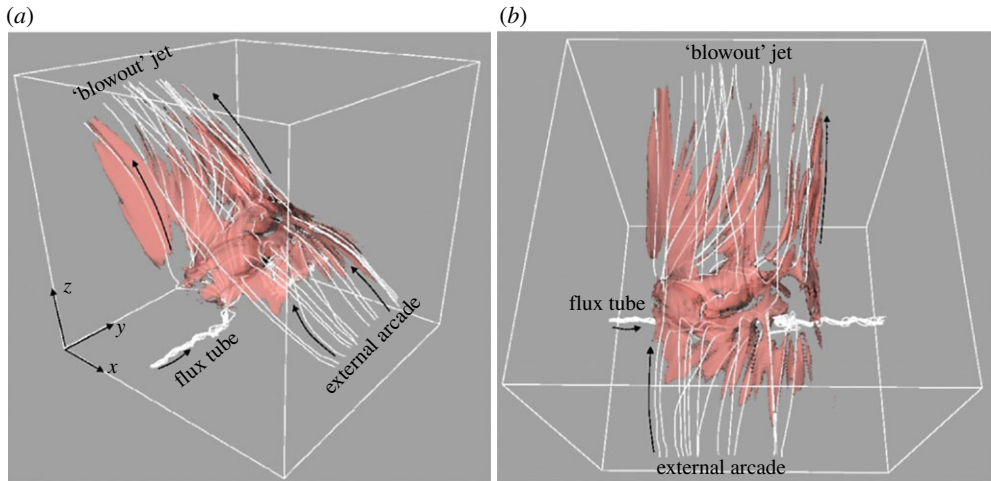
Figure 10. Side-view (*a*) and top view (*b*) of the 3D fieldline topology and velocity (isosurface greater than or equal to 200 km s^{-1}) during the blowout jet emission (*t* = 54 min). The direction of the fieldlines is shown by the (black) arrows [99]. (Online version in colour.)
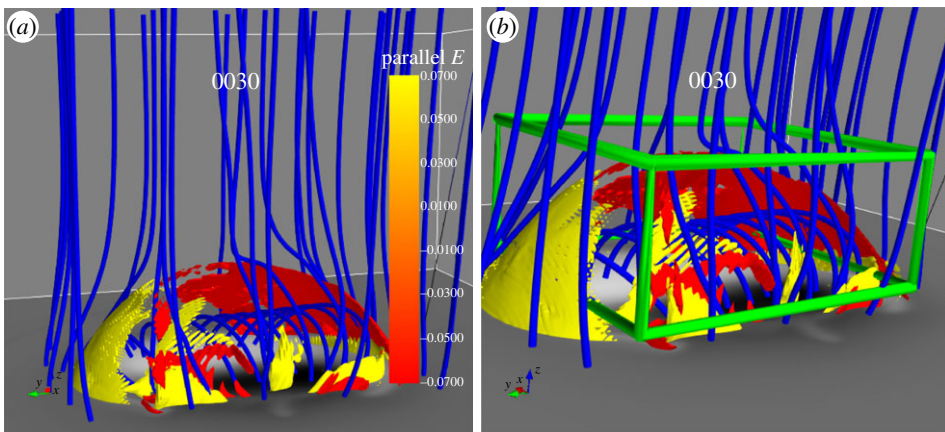

Figure 11. MHD simulations, zoom into the coronal part: (*a*) Magnetic field lines (blue tubes), together with an iso-contour plot of the parallel electric field (red and yellow 3D-surfaces). At the bottom *x*-*y*-plane, the photospheric component B_z is shown as a 2D filled contour plot. (*b*) As left, zoomed, and the region in which the spatial initial conditions for the particles are chosen is out-lined by a green cube [106].

same range than those that stay inside, although with a modulated power-law tail that is steeper, with index −2.98 at the highest energies (the fit is not shown).

The energy distribution of the leaving particles shows a functional form at low energies (between 0.1 and 10 keV) that is reminiscent of a Maxwellian, and a respective fit reveals a temperature of about 13.3 keV (see figure 12, the fit itself is not shown). Although the statistics are not very good, we can interpret these particles as belonging to a super-hot population. It is to be noted though that the energies are monitored at different times for each particle, so the distribution is asynchronous.

For the particles that stay inside, the Maxwellian shape of the energy distribution is well preserved at low energies, and there is heating from the initial 0.24 keV to 0.50 keV after 0.1 s, as the Maxwellian fit in figure 12 reveals.
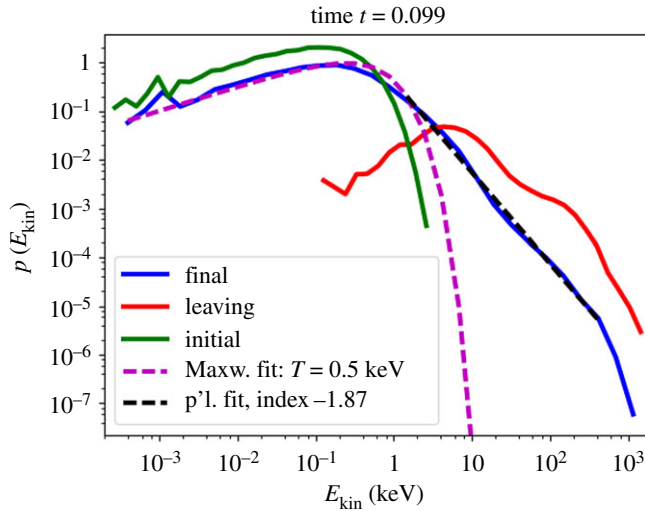
Figure 12. Snapshot 30: Kinetic energy distribution of electrons after $\approx 0.1\,$s, without collisions, together with a fit at the low energy, Maxwellian part and the high energy, power-law part, the initial distribution and the distribution of the leaving particles (for every particle at the time it leaves) [106]. (Online version in colour.)

As shown in [106], the distribution of energy increments has a power-law tail, as in the case of strong turbulence reported above [76], so that in the case of emerging flux, the transport in energy space is also of fractional nature.

6. Acceleration of particles by coronal mass ejection-driven shocks

One of the prominent acceleration mechanisms in astrophysics is shock waves. The acceleration of particles in shocks, developed by the eruption of unstable magnetic structures interacting with the ambient magnetic field inside the solar corona, is still an open problem. We are still lacking a clear model of the shock driven by a CME near the Sun, even if shock acceleration near the Sun appears to be the most promising acceleration mechanism for SEPs [107].

The theory of shock acceleration has been developed in relatively simple magnetic topologies of planar shocks. The angle between the direction of the ambient magnetic field upstream of the shock with the velocity of propagation of the shock is an important parameter for the acceleration process. When the shock is propagating along the direction of the magnetic field (parallel shock), the acceleration is due to the trapping of particles around the shock discontinuity by weak turbulence upstream and downstream. This mechanism is called diffusive shock acceleration (DSA) and has been analysed extensively in the current literature [108–111].

The mechanism of particle acceleration by shocks propagating perpendicular to the upstream magnetic field is different and relies mainly on the direct acceleration of particles drifting along the convective electric field $\mathbf{E} = -\mathbf{U} \times \mathbf{B}$ [112,113]. It is obvious that such a clear division of the two processes in realistic shocks travelling inside the solar corona is impossible, so the mixing of the two in a strongly turbulent plasma is more relevant and important.

Recently, a departure from the traditional approach was made by assuming that the turbulence upstream and downstream can reach very high amplitudes, $(\Delta B/B) >> 1$, and turbulent reconnection will set in [49,50]. This is true especially when a CME and the shock are propagating against a preexisting turbulent magnetic field or ambient magnetic structures, like the termination shock [114]. Yang *et al.* [115] simulated the interaction of the turbulent SW with the Earth's magnetic field using 3D Particle In Cell simulations. The CME-driven shocks have many similarities with the Earth's bow shock. Garrel *et al.* [52] discuss the flowing question: If

(a)   (b)
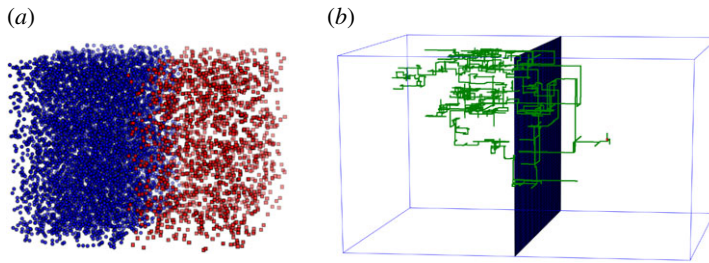
Figure 13. (*a*) Small version of the simulation box with the planar shock wave in the middle. The strongly turbulent environments upstream and downstream are acting as active scatterers. Particles not only return back to the shock, as in the case of the traditional DSA model but also gain energy upstream and downstream. (*b*) Trajectory of a typical particle inside the simulation box. [52].

large amplitude magnetic disturbances are present upstream and downstream of a shock then will turbulent reconnection set in and participate not only in the elastic scattering of particles but also in their heating and acceleration (see also [51])? Garrel *et al.* demonstrate that large amplitude magnetic disturbances and UCS, spontaneously formed in the strong turbulence in the vicinity of a shock, can accelerate particles as efficiently as DSA in large-scale systems and on long time scales (figure 13). They show that the asymptotic energy distribution of particles accelerated by the combined action of DSA and turbulent reconnection has very similar characteristics with the one due to DSA alone, but the synergy of DSA with turbulent reconnection is much more efficient: the acceleration time is an order of magnitude shorter and the maximum energy reached two orders of magnitude higher. They claim that DSA is the dominant acceleration mechanism in a short period before turbulent reconnection is established, and then strong turbulence will dominate the heating and acceleration of the particles. In other words, the eruptive large-scale magnetic structure and the shock formed ahead of a CME act as the mechanism to set up a strongly turbulent environment, in which the acceleration mechanism will ultimately be the synergy of DSA and turbulent reconnection.

7. Discussion

We can now pose an important question: If the standard flare cartoon is not a realistic representation of the physical processes related to solar eruptions, what will be its alternative?

The data-driven approach presented in §3 is much closer to a realistic representation of how solar eruptions spontaneously form current sheets in different parts of the stressed and twisted large-scale magnetic topology. The evolution of the large-scale current sheets presented in §5 shows how a fragmenting current sheet drives strong turbulence locally. The distinction of strong and weak turbulence and their efficiency in accelerating electrons and ions was analysed in §4. Combining the findings of these sections, we can redefine the term 'flare', as appearing in several articles studying impulsive SEP events, with the phrase 'impulsive energy release by the spontaneous formation of current sheets that fragment and form a strongly turbulent environment locally'.

In §6, we analyse the heating and acceleration of particles in shocks formed ahead of the CME and propagating inside the SW, which is always in the sate of strong turbulence. In many ways, the CME-driven shock is similar to the Earth's bow shock and departs from the simple model of the diffusive shock acceleration since the scattering of the particles upstream and downstream accelerates the particles as well.

Flare and CME-driven shocks rely on strong turbulence in order to heat and accelerate the plasma particles. The driver of the strong turbulence in the case of a 'flare' is the large-scale current sheet formed spontaneously in the low corona and fragmenting impulsively, and in the case of CME-driven shocks, the driver is the SW.

Let us now return to the key observational points mentioned in §2 and try to connect them with the theoretical arguments presented above.

— The impulsive-flare-related SEP events are associated with localized sources close to the Sun. Gradual-CME-related SEP events are usually determined at widely separated locations in the heliosphere.

— SEP events with characteristics resembling impulsive events can also be detected over a wide longitudinal range.

— The simplistic dichotomy of the SEP events into impulsive and gradual is not present in all SEP events.
The model presented here supports the view that the spontaneous formation of current sheets with different scales will take place in different parts of the large-scale erupting structure. Therefore, the impulsive injection of particles from many localized volumes, which are widely separated in space, should be expected. The CME-driven shock will be present in most eruptions and can also efficiently accelerate ions and electrons, as efficiently as a 'flare', as we have shown in §6. So the dichotomy between impulsive and gradual events depends mainly on the magnetic topology and the transport properties of the particles inside the complex and turbulent magnetic structures. In the erupting structure, the strong turbulence driven by the fragmented current sheet (impulsive SEP events) and the shock (gradual SEP events) will coexist.

— Observations are consistent with the acceleration process occurring over a wide range of longitudes rather than a small source region, and the accelerated particles could be transported before being injected at distant longitudes.
This is an important point and should be analysed in future studies. How the strongly turbulent plasma and the stochastic field lines generated by the current fragmentation will influence the anomalous transport of particles from the low corona to the interplanetary space remains an open problem.

— The comparison between CME or shock parameters and SEP properties show significant correlations, better than the correlations with flare parameters.
The eruptive magnetic structures forming a shock ahead of the CME will transport the accelerated particles in the interplanetary space much more easily than the impulsive events hidden inside the complex magnetic topology and forming current sheets.

— SEP events, either gradual or impulsive, were found to have high association with both type III and type II radio bursts.
Strong turbulence accelerates very efficiently both electrons and ions. The only difference is in the acceleration time, as the acceleration time for ions is ten times longer. We then expect that type III radio bursts will always be injected at the strongly turbulent locations associated with the fragmented current sheet. The type II radio burst will always be present when shocks are formed ahead of the CME. The fact that we do not always detect them is mainly due to observational limitations.

— Gradual events are generally considered to have a composition similar to that of the corona or SW, while impulsive events typically have enhanced element and isotope ratios.
We did not address this very important and crucial issue in this review, since the efficiency of strong turbulence in the acceleration of particles with different elemental abundances and isotopes has not been studied yet.

— The energy spectra based on the GLE show a double power-law, with the break between 2 and 50 MeV.
This observation is not only related with the sources of SEP events. The transport and acceleration of particles in the IP space is crucial and still remains an open problem. In §§4–6, we have reported the expected power low slopes of the accelerated particles in the coronal sources.

— Observations have revealed that most of the SEP events are associated with both flares and CMEs. Several intense flares that seem not to be accompanied by a CME were also lacking SEPs.
We claim that these peculiarities are related with the geometrical characteristics of the erupting magnetic topology and the anomalous transport of particles in the IP space.

8. Summary

In the current literature, the sources of SEPs remain confined to simple sketches and many assumptions based on monolithic current sheets, weak turbulence theory, and shocks travelling in ordered magnetic topologies, forming quasi-parallel or quasi-perpendicular shocks. The acceleration mechanisms are analysed separately from the evolving and dynamic magnetic structures in an eruptive magnetic topology.

In this review, we propose a different approach based on the recent developments in the study of eruptive magnetic structures and the analysis of particle acceleration in strongly turbulent plasmas. We claim that we cannot develop a realistic model for the sources of SEP events if the eruptive 3D magnetic topology remains on the level of simple sketches.

We suggest that the recent 3D data-driven studies of eruptive phenomena, based on the initialization of resistive 3D MHD codes with nonlinear force-free extrapolations of the observed magnetograms of specific ARs, driven by the turbulent photospheric activity [58,102,116], is clearly closer to reality.

It is clear that an eruptive realistic topology naturally forms reconnecting current sheets on all scales, and the large-scale reconnecting current sheets fragment, generating a distribution of strongly turbulent locations along the 3D structure. The fragmented large-scale current sheets and the interaction of the unstable magnetic structures form a turbulent reconnecting environment (a mixture of large-scale magnetic fluctuations and reconnecting current sheets) along the erupting magnetic structure. Emerging magnetic flux will also initially form large-scale reconnecting current sheets, which will fragment, forming a strongly turbulent environment and large-scale jets.

The CME-driven shock follows the same evolution as the main body of the eruptive structure. The presence of turbulent reconnection ahead (SW) and behind the shock play a key role in the long-lasting acceleration of ions and electrons. Karimabaldi *et al.* [115,117] proposed that the shock is linked with turbulence and reconnecting current sheets in a strongly turbulent environment.

How particles are accelerated in a strongly turbulent environment is a new topic that is under development in the current literature [71]. The main characteristic of the interaction of ions and electrons with a strongly turbulent plasma is the intense heating and the formation of power-law tails. The energy transport properties of the energized particles inside a strongly turbulent environment differ radically from the standard Fokker–Planck approach, since the interaction of the particles with strong turbulence is anomalous, and it can be described with a FTE [76,118].

We left outside our discussion in this review an important question: Can strong turbulence explain the abundance of elements and isotopes in SEPs? We hope that this question will be analysed soon in the context of strongly turbulent acceleration. A key observation, which we hope will be addressed properly with the Solar Probe, is the relative role of strong turbulence versus shock acceleration in the vicinity of the CME-driven shock front, close to the solar corona. Are phenomena present that are similar to the ones observed in the Earth's bow shock/magnetosphere?

Closing this review, it is important to stress once again that there is a close link between the acceleration mechanisms and the evolving large-scale erupting magnetic topology. The evolving topology is hosting the particular acceleration mechanisms through the distributed energy release sites along the large-scale structure.

References

1. Reames DV. 1995 Solar energetic particles: a paradigm shift. *Rev. Geophys.* **33**, 585–589. (doi:10.1029/95RG00188)
2. Klein KL, Trottet G. 2001 The origin of solar energetic particle events: coronal acceleration versus shock wave acceleration. *Space Sci. Rev.* **95**, 215–225. (doi:10.1023/A:1005236400689)
3. Lee MA. 2005 Coupled hydromagnetic wave excitation and ion acceleration at an evolving coronal/interplanetary shock. *Astrophys. J. Suppl.* **158**, 38–67. (doi:10.1086/428753)
4. Petrosian V. 2016 Particle acceleration in solar flares and associated CME shocks. *Astrophys. J.* **830**, 28. (doi:10.3847/0004-637X/830/1/28)
5. Petrosian V. 2012 Stochastic acceleration by turbulence. *Space Sci. Rev.* **173**, 535–556. (doi:10.1007/s11214-012-9900-6)
6. Cargill P, Vlahos L, Baumann G, Drake J, Nordlund Å. 2012 Current fragmentation and particle acceleration in solar flares. *Space Sci. Rev.* **173**, 223–245. (doi:10.1007/s11214-012-9888-y)
7. Reames DV. 1999 Particle acceleration at the Sun and in the heliosphere. *Space Sci. Rev.* **90**, 413–491. (doi:10.1023/A:1005105831781)
8. Miller JA, Cargill PJ, Emslie AG, Holman GD, Dennis BR, LaRosa TN, Winglee RM, Benka SG, Tsuneta S. 1997 Critical issues for understanding particle acceleration in impulsive solar flares. *J. Geoph. Res.* **102**, 14631–14660. (doi:10.1029/97JA00976)
9. Aschwanden MJ. 2002 Particle acceleration and kinematics in solar flares - a synthesis of recent observations and theoretical concepts (invited review). *Space Sci. Rev.* **101**, 1–227. (doi:10.1023/A:1019712124366)
10. Krauss-Varban D. 2010 Particle acceleration in shocks, p. 209.
11. Lee MA, Mewaldt RA, Giacalone J. 2012 Shock acceleration of ions in the heliosphere. *Space Sci. Rev.* **173**, 247–281. (doi:10.1007/s11214-012-9932-y)
12. Desai M, Giacalone J. 2016 Large gradual solar energetic particle events. *Living Rev. Sol. Phys.* **13**, 3. (doi:10.1007/s41116-016-0002-5)
13. Archontis V, Syntelis P. 2019 The emergence of magnetic flux and its role on the onset of solar dynamic events. *Phil. Trans. R. Soc. A* **377**, 20180387. (doi:10.1098/rsta.2018.0387)
14. Inoue S. 2016 Magnetohydrodynamics modeling of coronal magnetic field and solar eruptions based on the photospheric magnetic field. *Prog. Earth Planet. Sci.* **3**, 19. (doi:10.1186/s40645-016-0084-7)
15. Belov A, Garcia H, Kurt V, Mavromichalaki H, Gerontidou M. 2005 Proton enhancements and their relation to the X-ray flares during the three last solar cycles. *Solar Phys.* **229**, 135–159. (doi:10.1007/s11207-005-4721-3)
16. Anastasiadis A, Lario D, Papaioannou A, Kouloumvakos A, Vourlidas A. 2019 Solar energetic particles in the inner heliosphere: status and open questions. *Phil. Trans. R. Soc. A* **377**, 20180100. (doi:10.1098/rsta.2018.0100)
17. Richardson IG *et al.* 2014 25 MeV proton events observed by the high energy telescopes on the STEREO A and B spacecraft and/or at earth during the first seven years of the STEREO mission. *Solar Phys.* **289**, 3059–3107. (doi:10.1007/s11207-014-0524-8)
18. Wiedenbeck ME, Mason GM, Cohen CMS, Nitta NV, Gómez-Herrero R, Haggerty DK. 2013 Observations of solar energetic particles from ^{3}He-rich events over a wide range of heliographic longitude. *Astrophys. J.* **762**, 54. (doi:10.1088/0004-637X/762/1/54)
19. Rouillard AP *et al.* 2012 The longitudinal properties of a solar energetic particle event investigated using modern solar imaging. *Astrophys. J.* **752**, 44. (doi:10.1088/0004-637X/752/1/44)
20. Lario D, Raouafi NE, Kwon RY, Zhang J, Gómez-Herrero R, Dresing N, Riley P. 2014 The solar energetic particle event on 2013 April 11: an investigation of its solar origin and longitudinal spread. *Astrophys. J.* **797**, 8. (doi:10.1088/0004-637X/797/1/8)
21. Kouloumvakos A, Patsourakos S, Nindos A, Vourlidas A, Anastasiadis A, Hillaris A, Sandberg I. 2016 Multi-viewpoint observations of a widely distributed solar energetic

particle event: the role of euv waves and white-light shock signatures. *Astrophys. J.* **821**, 31. (doi:10.3847/0004-637X/821/1/31)

22. Lario D *et al.* 2016 Longitudinal properties of a widespread solar energetic particle event on 2014 february 25: evolution of the associated CME shock. *Astrophys. J.* **819**, 72. (doi:10.3847/0004-637X/819/1/72)

23. Lario D *et al.* 2017 The solar energetic particle event of 2010 August 14: connectivity with the solar source inferred from multiple spacecraft observations and modeling. *Astrophys. J.* **838**, 51. (doi:10.3847/1538-4357/aa63e4)

24. Kwon RY, Vourlidas A. 2018 The density compression ratio of shock fronts associated with coronal mass ejections. *J. Space Weather Space Clim.* **8**, A08. (doi:10.1051/swsc/2017045)

25. Park J, Innes DE, Bucik R, Moon YJ. 2013 The source regions of solar energetic particles detected by widely separated spacecraft. *Astrophys. J.* **779**, 184. (doi:10.1088/0004-637X/779/2/184)

26. Prise AJ, Harra LK, Matthews SA, Long DM, Aylward AD. 2014 An investigation of the CME of 3 November 2011 and its associated widespread solar energetic particle event. *Solar Phys.* **289**, 1731–1744. (doi:10.1007/s11207-013-0435-0)

27. Park J, Innes DE, Bucik R, Moon YJ, Kahler SW. 2015 Study of solar energetic particle associations with coronal extreme-ultraviolet waves. *Astrophys. J.* **808**, 3. (doi:10.1088/0004-637X/808/1/3)

28. Miteva R, Klein KL, Kienreich I, Temmer M, Veronig A, Malandraki OE. 2014 Solar energetic particles and associated EIT disturbances in solar cycle 23. *Solar Phys.* **289**, 2601–2631. (doi:10.1007/s11207-014-0499-5)

29. Kahler SW, Reames DV, Burkepile JT. 2000 A role for ambient energetic particle intensities in shock acceleration of solar energetic particles. In *High energy solar physics workshop - anticipating hess!* (eds R Ramaty, N Mandzhavidze). *Astronomical Society of the Pacific Conference Series*, no. 206. p. 468.

30. Kahler SW. 2001 The correlation between solar energetic particle peak intensities and speeds of coronal mass ejections: effects of ambient particle intensities and energy spectra. *J. Geophys. Res.* **106**, 20 947–20 956. (doi:10.1029/2000JA002231)

31. Kahler SW, Vourlidas A. 2005 Fast coronal mass ejection environments and the production of solar energetic particle events. *J. Geophys. Res.* **110**, A12S01. (doi:10.1029/2005JA011073)

32. Kahler SW, Vourlidas A. 2013 A comparison of the intensities and energies of gradual solar energetic particle events with the dynamical properties of associated coronal mass ejections. *Astrophys. J.* **769**, 143. (doi:10.1088/0004-637X/769/2/143)

33. Richardson IG, von-Rosenvinge TT, Cane HV. 2015 The properties of solar energetic particle event-associated coronal mass ejections reported in different CME catalogs. *Solar Phys.* **290**, 1741–1759. (doi:10.1007/s11207-015-0701-4)

34. Papaioannou A, Sandberg I, Anastasiadis A, Kouloumvakos A, Georgoulis MK, Tziotziou K, Tsiropoula G, Jiggens P, Hilgers A. 2016 Solar flares, coronal mass ejections and solar energetic particle event characteristics. *J. Space Weather Space Clim.* **6**, A42. (doi:10.1051/swsc/2016035)

35. Ontiveros V, Vourlidas A. 2009 Quantitative measurements of coronal mass ejection-driven shocks from LASCO observations. *Astrophys. J.* **693**, 267–275. (doi:10.1088/0004-637X/693/1/267)

36. Bemporad A, Susino R, Lapenta G. 2014 Plasma physical parameters along coronal-mass-ejection-driven shocks. I. Ultraviolet and white-light observations. *Astrophys. J.* **784**, 102. (doi:10.1088/0004-637X/784/2/102)

37. Kouloumvakos A, Patsourakos S, Hillaris A, Vourlidas A, Preka-Papadema P, Moussas X, Caroubalos C, Tsitsipis P, Kontogeorgos A. 2014 CME expansion as the driver of metric type II shock emission as revealed by self-consistent analysis of high-cadence EUV images and radio spectrograms. *Solar Phys.* **289**, 2123–2139. (doi:10.1007/s11207-013-0460-z)

38. Kozarev KA, Evans RM, Schwadron NA, Dayeh MA, Opher M, Korreck KE, van der Holst B. 2013 Global numerical modeling of energetic proton acceleration in a coronal mass ejection traveling through the solar corona. *Astrophys. J.* **778**, 43. (doi:10.1088/0004-637X/778/1/43)

39. Kozarev KA, Raymond JC, Lobzin VV, Hammer M. 2015 Properties of a coronal shock wave as a driver of early SEP acceleration. *Astrophys. J.* **799**, 167. (doi:10.1088/0004-637X/799/2/167)

40. Rouillard AP, Plotnikov I, Pinto RF, Tirole M, Lavarra M, Zucca P, Vainio R, Tylka AJ, Vourlidas A, De-Rosa ML, Linker J, Warmuth A, Mann G, Cohen CMS, Mewaldt RA.

41. Afanasiev A, Vainio R, Rouillard AP, Battarbee M, Aran A, Zucca P. 2018 Modelling of proton acceleration in application to a ground level enhancement. *Astron. Astrophys.* **614**, A4. (doi:10.1051/0004-6361/201731343)

42. Kouloumvakos A, Rouillard AP, Wu Y, Vainio R, Vourlidas A, Plotnikov I, Afanasiev A, Hakan O. 2019 Connecting the properties of coronal shock waves with those of solar energetic particles. (Accepted by *The Astrophysics Journal*).

43. Cane HV, Richardson IG, von Rosenvinge TT. 2010 A study of solar energetic particle events of 1997–2006: their composition and associations. *J. Geophys. Res.* **115**, A08101. (doi:10.1029/2009JA014848)

44. Miteva R, Klein KL, Samwel SW, Nindos A, Kouloumvakos A, Reid H. 2013 Radio signatures of solar energetic particles during the 23rd solar cycle. *Cent. Eur. Astrophys. Bull.* **37**, 541–553.

45. Kouloumvakos A, Nindos A, Valtonen E, Alissandrakis CE, Malandraki O, Tsitsipis P, Kontogeorgos A, Moussas X, Hillaris A. 2015 Properties of solar energetic particle events inferred from their associated radio emission. *Astron. Astrophys.* **580**, A80. (doi:10.1051/0004-6361/201424397)

46. Reames DV. 2018 Abundances, ionization states, temperatures, and FIP in solar energetic particles. *Space Sci. Rev.* **214**, 61. (doi:10.1007/s11214-018-0495-4)

47. Mewaldt RA, Looper MD, Cohen CMS, Haggerty DK, Labrador AW, Leske RA, Mason GM, Mazur JE, von Rosenvinge TT. 2012 Energy spectra, composition, and other properties of ground-level events during Solar Cycle 23. *Space Sci. Rev.* **171**, 97–120. (doi:10.1007/s11214-012-9884-2)

48. Mewaldt RA, Cohen CMS, Mason GM, von Rosenvinge TT, Leske RA, Luhmann JG, Odstrcil D, Vourlidas A. 2013 Solar energetic particles and their variability from the sun and beyond. *Solar Wind* **13**, 1539, 116–121. (doi:10.1063/1.4811002)

49. Zank GP *et al.* 2015 Diffusive shock acceleration and reconnection acceleration processes. *Astrophys. J.* **814**, 137. (doi:10.1088/0004-637X/814/2/137)

50. le-Roux JA, Zank GP, Webb GM, Khabarova OV. 2016 Combining diffusive shock acceleration with acceleration by contracting and reconnecting small-scale flux ropes at heliospheric shocks. *Astrophys. J.* **827**, 47. (doi:10.3847/0004-637X/827/1/47)

51. Afanasiev A, Vainio R, Kocharov L. 2014 The effect of stochastic re-acceleration on the energy spectrum of shock-accelerated protons. *Astrophys. J.* **790**, 36. (doi:10.1088/0004-637X/790/1/36)

52. Garrel C, Vlahos L, Isliker H, Pisokas T. 2018 Diffusive shock acceleration and turbulent reconnection. *Mon. Not. R. Astron. Soc.* **478**, 2976–2986. (doi:10.1093/mnras/sty1260)

53. Wang Y, Zhang J. 2007 A comparative study between eruptive X-class flares associated with coronal mass ejections and confined X-class flares. *Astrophys. J.* **665**, 1428–1438. (doi:10.1086/519765)

54. Klein KL, Trottet G, Klassen A. 2010 Energetic particle acceleration and propagation in strong CME-less flares. *Solar Phys.* **263**, 185–208. (doi:10.1007/s11207-010-9540-5)

55. Klein KL, Trottet G, Samwel S, Malandraki O. 2011 Particle acceleration and propagation in strong flares without major solar energetic particle events. *Solar Phys.* **269**, 309–333. (doi:10.1007/s11207-011-9710-0)

56. Kahler SW, Cliver EW, Cane HV, McGuire RE, Stone RG, Sheeley NR Jr. 1986 Solar filament eruptions and energetic particle events. *Astrophys. J.* **302**, 504–510. (doi:10.1086/164009)

57. Kliem B, Su YN, van Ballegooijen AA, DeLuca EE. 2013 Magnetohydrodynamic modeling of the solar eruption on 2010 April 8. *Astrophys. J.* **779**, 129. (doi:10.1088/0004-637X/779/2/129)

58. Inoue S, Shiota D, Bamba Y, Park SH. 2018 Magnetohydrodynamic modeling of a solar eruption associated with an X9.3 flare observed in the active region 12673. *Astrophys. J.* **867**, 83. (doi:10.3847/1538-4357/aae079)

59. Jiang C, Wu ST, Feng X, Hu Q. 2016 Data-driven magnetohydrodynamic modelling of a flux-emerging active region leading to solar eruption. *Nat. Commun.* **7**, 11522. (doi:10.1038/ncomms11522)

60. Onofri M, Isliker H, Vlahos L. 2006 Stochastic acceleration in turbulent electric fields generated by 3D reconnection. *Phys. Rev. Lett.* **96**, 151102. (doi:10.1103/PhysRevLett.96.151102)

61. Dahlin JT, Drake JF, Swisdak M. 2015 Electron acceleration in three-dimensional magnetic reconnection with a guide field. *Phys. Plasmas* **22**, 100704. (doi:10.1063/1.4933212)
62. Melrose DB. 2009 Acceleration mechanisms. ArXiv e-prints.
63. Fermi E. 1949 On the origin of the cosmic radiation. *Phys. Rev.* **75**, 1169–1174. (doi:10.1103/PhysRev.75.1169)
64. Longair MS. 2011 *High energy astrophysics*. Cambridge, UK: Cambridge University Press.
65. Davis L. 1956 Modified fermi mechanism for the acceleration of cosmic rays. *Phys. Rev.* **101**, 351–358. (doi:10.1103/PhysRev.101.351)
66. Parker EN, Tidman DA. 1958 Suprathermal particles. *Phys. Rev.* **111**, 1206–1211. (doi:10.1103/PhysRev.111.1206)
67. Tverskoi BA. 1967 The influence of corpuscular radiation on the circumterrestrial cloud. *Sov. Astron.* **10**, 1031.
68. Kulsrud RM, Ferrari A. 1971 The relativistic quasilinear theory of particle acceleration by hydromagnetic turbulence. *Astrophys. Space Sci.* **12**, 302–318. (doi:10.1007/BF0065 1420)
69. Achterberg A. 1981 On the nature of small amplitude fermi acceleration. *Astron. Astrophys.* **97**, 259–264.
70. Schlickeiser R. 1989 Cosmic-ray transport and acceleration. I - derivation of the kinetic equation and application to cosmic rays in static cold media. II - cosmic rays in moving cold media with application to diffusive shock wave acceleration. *Astrophys. J.* **336**, 243–293. (doi:10.1086/167009)
71. Vlahos L, Isliker H. 2019 Particle acceleration and heating in a turbulent solar corona. *Plasma Phys. Controlled Fusion* **61**, 014020.
72. Matthaeus WH, Lamkin SL. 1986 Turbulent magnetic reconnection. *Phys. Fluids* **29**, 2513–2534. (doi:10.1063/1.866004)
73. Lazarian A, Vishniac ET. 1999 Reconnection in a weakly stochastic field. *Astrophys. J.* **517**, 700–718. (doi:10.1086/307233)
74. Lazarian A, Eyink G, Vishniac E, Kowal G. 2015 Turbulent reconnection and its implications. *Phil. Trans. R. Soc. Lond. A* **373**, 20140144. (doi:10.1098/rsta.2014.0144)
75. Matthaeus WH, Wan M, Servidio S, Greco A, Osman KT, Oughton S, Dmitruk P. 2015 Intermittency, nonlinear dynamics and dissipation in the solar wind and astrophysical plasmas. *Phil. Trans. R. Soc. Lond. A* **373**, 20140154. (doi:10.1098/rsta.2014.0154)
76. Isliker H, Vlahos L, Constantinescu D. 2017 Fractional transport in strongly turbulent plasmas. *Phys. Rev. Lett.* **119**, 045101. (doi:10.1103/PhysRevLett.119.045101)
77. Dmitruk P, Matthaeus WH, Seenu N. 2004 Test particle energization by current sheets and nonuniform fields in magnetohydrodynamic turbulence. *Astrophys. J.* **617**, 667–679. (doi:10.1086/425301)
78. Arzner K, Vlahos L. 2004 Particle acceleration in multiple dissipation regions. *Astrophys. J. Lett.* **605**, L69.
79. Boyd JP. 2001 *Chebyshev and fourier spectral methods*. New York, NY: Dover Publications.
80. Gottlieb S, Shu CW. 1998 Total variation diminishing Runge-Kutta schemes. *Math. Computat.* **67**, 73–85. (doi:10.1090/S0025-5718-98-00913-2)
81. Biskamp D, Welter H. 1989 Dynamics of decaying two-dimensional magnetohydrodynamic turbulence. *Phys. Fluids B* **1**, 1964–1979. (doi:10.1063/1.859060)
82. Arzner K, Knaepen B, Carati D, Denewet N, Vlahos L. 2006 The effect of coherent structures on stochastic acceleration in MHD turbulence. *Astrophys. J.* **637**, 322–332. (doi:10.1086/498341)
83. Servidio S, Matthaeus WH, Shay MA, Cassak PA, Dmitruk P. 2009 Magnetic reconnection in two-dimensional magnetohydrodynamic turbulence. *Phys. Rev. Lett.* **102**, 115003. (doi:10.1103/PhysRevLett.102.115003)
84. Servidio S, Matthaeus WH, Shay MA, Dmitruk P, Cassak PA, Wan M. 2010 Statistics of magnetic reconnection in two-dimensional magnetohydrodynamic turbulence. *Phys. Plasmas* **17**, 032315. (doi:10.1063/1.3368798)
85. Servidio S, Dmitruk P, Greco A, Wan M, Donato S, Cassak PA, Shay MA, Carbone V, Matthaeus WH. 2011 Magnetic reconnection as an element of turbulence. *Nonlinear Process. Geophys.* **18**, 675–695. (doi:10.5194/npg-18-675-2011)

86. Uritsky VM, Pouquet A, Rosenberg D, Mininni PD, Donovan EF. 2010 Structures in magnetohydrodynamic turbulence: detection and scaling. *Phys. Rev. E* **82**, 056326. (doi:10.1103/PhysRevE.82.056326)

87. Zhdankin V, Uzdensky DA, Perez JC, Boldyrev S. 2013 Statistical analysis of current sheets in three-dimensional magnetohydrodynamic turbulence. *Astrophs. J.* **771**, 124. (doi:10.1088/0004-637X/771/2/124)

88. Ambrosiano J, Matthaeus WH, Goldstein ML, Plante D. 1988 Test particle acceleration in turbulent reconnecting magnetic fields. *J. Geophys. Res.: Space Phys.* **93**, 14 383–14 400.

89. Dmitruk P, Matthaeus W, Seenu N, Brown MR. 2003 Test particle acceleration in three-dimensional magnetohydrodynamic turbulence. *Astrophys. J. Lett.* **597**, L81. (doi:10.1086/379751)

90. Guo F, Liu YH, Daughton W, Li H. 2015 Particle acceleration and plasma dynamics during magnetic reconnection in the magnetically dominated regime. *Astrophys. J.* **806**, 167. (doi:10.1088/0004-637X/806/2/167)

91. Pisokas T, Vlahos L, Isliker H, Tsiolis V, Anastasiadis A. 2017 Stochastic Fermi energization of coronal plasma during explosive magnetic energy release. *Astrophys. J.* **835**, doi:10.3847/1538-4357/835/2/214)

92. Pisokas T, Vlahos L, Isliker H. 2018 Synergy of stochastic and systematic energization of plasmas during turbulent reconnection. *Astrophys. J.* **852**, 64. (doi:10.3847/1538-4357/aaa1e0)

93. Heyvaerts J, Priest ER, Rust DM. 1977 An emerging flux model for the solar phenomenon. *Astrophys. J.* **216**, 123–137. (doi:10.1086/155453)

94. Archontis V, Moreno-Insertis F, Galsgaard K, Hood A, O'Shea E. 2004 Emergence of magnetic flux from the convection zone into the corona. *Astron. Astrophys.* **426**, 1047–1063. (doi:10.1051/0004-6361:20035934)

95. Galsgaard K, Moreno-Insertis F, Archontis V, Hood A. 2005 A three-dimensional study of reconnection, current sheets, and jets resulting from magnetic flux emergence in the sun. *Astrophys. J.* **618**, L153–L156. (doi:10.1086/427872)

96. Archontis V, Moreno-Insertis F, Galsgaard K, Hood AW. 2005 The three-dimensional interaction between emerging magnetic flux and a large-scale coronal field: reconnection, current sheets, and jets. *Astrophys. J.* **635**, 1299–1318. (doi:10.1086/497533)

97. Archontis V, Hood AW. 2012 Magnetic flux emergence: a precursor of solar plasma expulsion. *Astron. Astrophys.* **537**, A62. (doi:10.1051/0004-6361/201116956)

98. Archontis V. 2012 Magnetic flux emergence and associated dynamic phenomena in the sun. *Phil. Trans. R. Soc. A* **370**, 3088–3113. (doi:10.1098/rsta.2012.0001)

99. Archontis V, Hood AW. 2013 A numerical model of standard to blowout jets. *Astrophys. J.* **769**, L21. (doi:10.1088/2041-8205/769/2/L21)

100. Moreno-Insertis F, Galsgaard K. 2013 Plasma jets and eruptions in solar coronal holes: a three-dimensional flux emergence experiment. *Astrophys. J.* **771**, 20. (doi:10.1088/0004-637X/771/1/20)

101. Karimabadi H, Lazarian A. 2013 Magnetic reconnection in the presence of externally driven and self-generated turbulence. *Phys. Plasmas* **20**, 112102. (doi:10.1063/1.4828395)

102. Jiang C, Wu ST, Feng X, Hu Q. 2016 Data-driven magnetohydrodynamic modelling of a flux-emerging active region leading to solar eruption. *Nat. Commun.* **7**, 11522. (doi:10.1038/ncomms11522)

103. Raouafi NE *et al.* 2016 Solar coronal jets: observations, theory, and modeling. *Space Sci. Rev.* **201**, 1–53. (doi:10.1007/s11214-016-0260-5)

104. Wyper PF, DeVore CR, Karpen JT, Lynch BJ. 2016 Three-dimensional simulations of tearing and intermittency in coronal jets. *Astrophys. J.* **827**, 4. (doi:10.3847/0004-637X/827/1/4)

105. Wyper PF, Antiochos SK, DeVore CR. 2017 A universal model for solar eruptions. *Nature* **544**, 452–455. (doi:10.1038/nature22050)

106. Isliker H, Archontis V, Vlahos L. Particle acceleration in regions of magnetic flux emergence. to be submited.

107. Lee MA, Mewaldt RA, Giacalone J. 2012 Shock acceleration of ions in the heliosphere. *Space Sci. Rev.* **173**, 247–281. (doi:10.1007/s11214-012-9932-y)

108. Burgess D, Scholer M. 2013 Microphysics of quasi-parallel shocks in collisionless plasmas. *Space Sci. Rev.* **178**, 513–533. (doi:10.1007/s11214-013-9969-6)

109. Caprioli D, Spitkovsky A. 2014 Simulations of ion acceleration at non-relativistic shocks. I. Acceleration efficiency. *Astrophys. J.* **783**, 91. (doi:10.1088/0004-637X/783/2/91)

110. Caprioli D, Spitkovsky A. 2014 Simulations of ion acceleration at non-relativistic shocks. II. Magnetic field amplification. *Astrophys. J.* **794**, 46. (doi:10.1088/0004-637X/794/1/46)

111. Caprioli D, Spitkovsky A. 2014 Simulations of ion acceleration at non-relativistic shocks. III. Particle diffusion. *Astrophys. J.* **794**, 47. (doi:10.1088/0004-637X/794/1/47)

112. Holman GD. 1985 Acceleration of runaway electrons and joule heating in solar flares. *Astrophys. J.* **293**, 584–594. (doi:10.1086/163263)

113. Sandroos A, Vainio R. 2006 Particle acceleration at shocks propagating in inhomogeneous magnetic fields. *Astron. Astrophys.* **455**, 685–695. (doi:10.1051/0004-6361:20054754)

114. Burgess D, Gingell PW, Matteini L. 2016 Multiple current sheet systems in the outer heliosphere: energy release and turbulence. *Astrophys. J.* **822**, 38. (doi:10.3847/0004-637X/822/1/38)

115. Yang Z, Huang C, Liu YD, Parks GK, Wang R, Lu Q, Hu H. 2016 Global explicit particle-in-cell simulations of the nonstationary bow shock and magnetosphere. *Astrophys. J. Suppl. Ser.* **225**, 13. (doi:10.3847/0067-0049/225/1/13)

116. Amari T, Canou A, Aly JJ, Delyon F, Alauzet F. 2018 Magnetic cage and rope as the key for solar eruptions. *Nature* **554**, 211–215. (doi:10.1038/nature24671)

117. Karimabadi H *et al.* 2014 The link between shocks, turbulence, and magnetic reconnection in collisionless plasmas. *Phys. Plasmas* **21**, 062308. (doi:10.1063/1.4882875)

118. Isliker H, Pisokas T, Vlahos L, Anastasiadis A. 2017 Particle acceleration and fractional transport in turbulent reconnection. ArXiv e-prints.